tvst

DOI: 10.1167/tvst.6.3.2

Article

Role of a Dual Splicing and Amino Acid Code in Myopia, Cone Dysfunction and Cone Dystrophy Associated with *L/M* Opsin Interchange Mutations

Scott H. Greenwald[1], James A. Kuchenbecker[1], Jessica S. Rowlan[1], Jay Neitz[1], and Maureen Neitz[1]

[1] Department of Ophthalmology, University of Washington, Seattle, WA, USA

Correspondence: Maureen Neitz, University of Washington School of Medicine Vision Sciences at South Lake Union/Ophthalmology, Box 358058, 750 Republican Street, Building E Room, Seattle, WA 98109. e-mail: mneitz@uw.edu

Received: 15 August 2016
Accepted: 2 February 2017
Published: 10 May 2017

Keywords: myopia; cone dystrophy; opsin mutations

Citation: Greenwald SH, Kuchenbecker JA, Rowlan JS, Neitz J, Neitz M. Role of a dual splicing and amino acid code in myopia, cone dysfunction and cone dystrophy associated with *L/M* opsin interchange mutations. Trans Vis Sci Tech. 2017;6(3):2, doi:10.1167/tvst.6.3.2

Purpose: Human long (*L*) and middle (*M*) wavelength cone opsin genes are highly variable due to intermixing. Two *L/M* cone opsin interchange mutants, designated *LIAVA* and *LVAVA*, are associated with clinical diagnoses, including red-green color vision deficiency, blue cone monochromacy, cone degeneration, myopia, and Bornholm Eye Disease. Because the protein and splicing codes are carried by the same nucleotides, intermixing *L* and *M* genes can cause disease by affecting protein structure and splicing.

Methods: Genetically engineered mice were created to allow investigation of the consequences of altered protein structure alone, and the effects on cone morphology were examined using immunohistochemistry. In humans and mice, cone function was evaluated using the electroretinogram (ERG) under *L/M*- or short (S) wavelength cone isolating conditions. Effects of *LIAVA* and *LVAVA* genes on splicing were evaluated using a minigene assay.

Results: ERGs and histology in mice revealed protein toxicity for the LVAVA but not for the LIAVA opsin. Minigene assays showed that the dominant messenger RNA (mRNA) was aberrantly spliced for both variants; however, the *LVAVA* gene produced a small but significant amount of full-length mRNA and *LVAVA* subjects had correspondingly reduced ERG amplitudes. In contrast, the *LIAVA* subject had no *L/M* cone ERG.

Conclusions: Dramatic differences in phenotype can result from seemingly minor differences in genotype through divergent effects on the dual amino acid and splicing codes.

Translational Relevance: The mechanism by which individual mutations contribute to clinical phenotypes provides valuable information for diagnosis and prognosis of vision disorders associated with *L/M* interchange mutations, and it informs strategies for developing therapies.

Introduction

During primate evolution, the control of spectral tuning is an obvious factor that drove the divergence of the long wavelength sensitive (*L*) and middle wavelength (*M*) opsin gene sequences (*OPN1LW* and *OPN1MW*, respectively). However, the presence of amino acid differences between the L and M opsins that are associated with very small or no spectral shifts suggests that their sequences also may be constrained by other aspects of protein structure and function besides those responsible for controlling the wavelength of peak absorption. Additional evolutionary constraints are imposed by signals within the coding regions that are important for regulating the proper splicing of precursor messenger RNA (pre-mRNA).[1] Although they originally were discovered in alternatively spliced exons, exon splicing enhancers and silencers (ESEs and ESSs) are now known to be ubiquitous so that the exon sequences represent overlaid splicing and amino acid codes.[2–4]

The *L* and *M* opsin genes of Old World nonhuman primates have stereotyped differences that presumably have been shaped by the dual evolutionary pressures of the superimposed exon splicing and amino acid

codes.[1,5] In contrast to other primates, humans show extreme variation in the nucleotide sequences of the *L* and *M* opsin genes. Almost always, genetic polymorphisms are assumed to be attributable to the pressure of selective advantage driving an increase in the frequency of the different variants in the population; however, this is not the case for the *L* and *M* opsin genes.[6] Their high homology and tandem arrangement on the X-chromosome have allowed for an extremely high mutation rate in which the sequences of the primordial *L* and *M* opsin genes have been interchanged.[6–9] Presumably, the strong "mutation pressure" associated with a high rate of producing *L*/*M* opsin gene interchange variants is counteracted in nonhuman primates by robust selection pressure against red-green color vision deficiencies, and this may explain the absence of *L* and *M* opsin sequence variability in those species. In contrast, selection against colorblindness apparently is relaxed in modern humans who, for example, do not rely on color vision to obtain food by hunting and gathering. Thus, the ongoing intermixing of the human *L* and *M* opsin genes is a purely degenerative process that is undoing evolution's handiwork in creating well-designed photopigments in the face of constraints on protein structure and function, as well as those associated with the control of pre-mRNA splicing. The result is that some combinations of individually benign nucleotide variations are associated with photoreceptor dysfunction, and cone opsin gene interchange variants are becoming recognized as important causes of vision loss.[6,10–18] Vision disorders frequently have been associated with two such variants, abbreviated *LIAVA* and *LVAVA*, for the amino acids specified by exon 3 codons 153, 171, 174, 178, and 180 where *L* is leucine, V is valine, I is isoleucine, and A is alanine.[10–12,14–18] However, the mechanism whereby these two variant opsin genes cause vision problems has not been clear. More generally, the wide diversity of phenotypes associated with "interchange variants" has been particularly difficult to explain, having been identified in individuals with a variety of clinical diagnoses including red-green color vision deficiency, blue cone monochromacy, high grade myopia, cone dysfunction, and cone dystrophy.[6,10–16]

We originally discovered *LVAVA* as being associated with Bornholm eye disease (BED),[16,18] which is characterized by color vision deficiency and high-grade myopia, and *LIAVA* as being associated with red-green color blindness.[10,12] The corresponding opsin gene haplotypes cause vision disorders when present in either the *L* or the *M* genes. *LVAVA* was originally identified in individuals with high myopia and color vision deficiencies, but the color vision defect was caused by a separate mutation.[18] Usually, only the first two opsin genes in the X-chromosome are expressed.[19] When an *LVAVA* opsin gene is present in one of the two expressed positions, and the other expressed position harbors a normal photopigment of contrasting type, it is reliably associated with very high myopia without color vision deficiency.[20]

In contrast, when one of the two expressed genes from the X-chromosome encodes *LIAVA* and the other encodes a normally functioning cone photopigment, dichromacy always is observed; however, the *LIAVA* opsin gene variant also can be associated with myopia, but to a much more variable degree than the *LVAVA* opsin gene variant. For example, for the patients reported by Patterson et al.,[18] the standard deviation (SD) for refractive error was more than 5 times higher (SD = 5.27 diopters) for patients with an *LIAVA* opsin gene variant than for patients with an *LVAVA* opsin gene variant (SD = 0.91 diopters).

Instead of patients with X-chromosome opsin gene arrays that are expected to transcribe either an *LIAVA* or *LVAVA* opsin gene in one submosaic of cones and a normal functioning opsin in a second submosaic, as for the Patterson et al. study,[18] here we studied human patients who were expected to transcribe only an *LVAVA* or only an *LIAVA* opsin gene variant in all cones that are normally *L* or *M*. These people would have been common red-green dichromats if their expressed gene produced a normal functioning photopigment; however, one received a clinical diagnosis of blue cone monochromacy, and the other two were diagnosed as having cone dystrophy. These individuals offered a unique opportunity to study the physiology and function of cones expressing these two disease-causing *L*/*M* interchange opsin genes and to understand the basis for the diverse symptoms associated with these mutations.

Recently, Ueyama et al.[15] and Gardner et al.[17] identified splicing defects for the exon 3 haplotypes that specify the *LIAVA* and *LVAVA* opsin variants.[15,17] This important observation underscores the fact that effects on splicing and on protein structure and function must be examined if the fundamental mechanism by which these and similar variants cause vision loss is to be understood and for developing gene-based therapies. Here, effects of *LIAVA* and *LVAVA* genes from human patients on splicing were evaluated using a minigene assay. We also performed cone-isolating electroretinograms (ERGs) on human patients with either the *LVAVA* or *LIAVA* opsin gene

variant in all L/M cones, and, therefore, their phenotypes reflect the combined effects of the splicing defect, which is associated with abnormally low levels of photopigment and the effects of the altered protein, at least to the extent that the altered protein is made.

The locations of the polymorphic amino acid positions encoded by the *LVAVA* and *LIAVA* haplotypes suggest an effect of amino acid sequence on function. That is, amino acid position 153 is immediately adjacent to the highly conserved "ionic lock" tripeptide comprised of residues 150, 151, and 152 that is crucial for photopigment function. In addition, residues 171, 174 and 178 all reside on the same surface of the fourth transmembrane α helix, each one turn down from the other, allowing for interactions that might affect function. Further support for the idea that these variants may be associated with protein function deficits comes from the observations that mutations at rhodopsin amino acid positions 137 and 164, which correspond to *L/M* opsin amino acid positions 153 and 180, respectively, cause retinitis pigmentosa.[21,22]

The effects of *L/M* interchange mutations on protein structure and function were examined separately from the effects due to splicing errors by creating three targeted gene replacement mouse lines. Each line expressed a modified *L* opsin complementary DNA (cDNA) variant specifying either the *LIAVA* or *LVAVA* *L/M* interchange mutant or a "normal" control *LIAIS* (S is serine) variant that is potentially the human primordial *L* opsin. The modified mouse opsin gene locus prevented the effects of the exon 3 sequence on splicing so that the phenotypes in the mice reflected only the effects of the specified photopigment variant. Importantly, these mutant opsin mouse models allowed the effects of protein structure and function to be separated from the effects of abnormally low amounts of photopigment associated with the splicing defect.

Evidence from experiments described here supports the idea that even though the LIAVA and LVAVA opsins differ by a single isoleucine-to-valine exchange at the amino acid level, they differ substantially at the level of protein structure and function and in the amount of full-length mRNA made. The combined effects translate into dramatically different disease phenotypes produced by the two *L/M* interchange variants. Understanding the contributions of the dual splicing and amino acid codes has important implications for the diagnosis, prognosis, and ultimately the treatment of the varied eye disorders associated with the *L/M* opsin interchange mutants. From these experiments, we have gained insights into how cone function and viability are affected by the amount of opsin produced and by changes in protein structure that lead to cone dystrophy. In addition, the experiments reported here provide insights into the fundamental causes of myopia in humans, which have far-reaching implications for understanding everyday juvenile onset myopia and how it might be mitigated.

Methods

Human Subjects

The Institutional Review Board of the University of Washington approved all experiments involving the use of human subjects. These experiments were conducted in accordance with the principles embodied in the Declaration of Helsinki.

A series of color vision tests was administered to each of the participants including the Richmond HRR 2012 edition, color matching on the Nagel Anomaloscope, Farnsworth D15, and Lanthony's desaturated D15 test. The Zeiss IOL Master (Carl Zeiss Meditec, Jena, Germany) was used to measure the axial length and corneal curvature of each eye, and from these data, the spherical equivalent refractive error (SER) was estimated. The Titmus test was used to measure the best corrected visual acuities. To verify the previously reported *L/M* opsin gene sequence information for each subject, we extracted DNA from fresh blood samples obtained from each subject and sequenced the *OPN1LW* and *OPN1MW* genes using previously described methods.[12] For subject 11-0271, the promoter of the *L* and *M* opsin genes also was sequenced according to a previously described method.[23] The opsin gene array structure was evaluated using a MassArray-based (Agena Bioscience, Inc., Hamburg, Germany) procedure that has been described in detail.[24] The exons and intron/exon junctions for the *S* cone opsin genes in subjects 10-0059 and 11-0115 were sequenced using previously described methods.[25,26]

Mice

Animal experiments conformed to the ARVO Animal Statement for the use of Animals in Ophthalmic and Vis Res. and were approved by the Animal Care and Use Committee at the University of Washington. Four lines of genetically modified mice were created by Ozgene, Inc. (Perth, Australia). The design of the modified X-chromosome opsin gene

locus used in three of the mouse lines has been described in detail previously.[27] Briefly, the region on mouse X-chromosome extending from nucleotide 71,378,135 through nucleotide 71,389,460 (numbers from the July 2007 assembly of the mouse genome, NCBI 57/mm9) was replaced with a segment of human *L* opsin cDNA from plasmid hs7 extending from the *Bbs*I site in exon 2 through nucleotide 1695 (fig. 7 reported by Nathans et al.[28]). Before incorporating into the targeting construct, the human *L* opsin cDNA was subjected to site directed mutagenesis as previously described[27] to: (1) alter exon 2 codons 58 and 52 so that the amino acids specified matched that of human L/M opsin, (2) alter codon 65 to encode the amino acid Threonine (T), typically found in human *L* opsin, and (3) alter the amino acids encoded by codons 153, 171, 174, 178, and 180 to specify either LVAVA, LIAVA, or LIAIS. In human *L* opsins, amino acid positions 111, 116, 230, 233, and 236 are variable, and for the three mouse lines generated here, the amino acids specified at these positions were I111, S116, I230, A233, and M236 (*M* is for methionine). Thus, the modified locus in each mouse line had only one intron, which separated exon 1 from the second exon that was a cDNA comprised of exon 2 through 6 and included the 3′ untranslated region of human *OPN1LW*. The modified X-chromosome locus and the transcribed product was confirmed for each line by direct sequencing of genomic DNA and direct sequencing of cDNA made from retinal mRNA.

The different lines of mice were bred to mice in which the short-wavelength sensitive opsin gene had been knocked-out ($Opn1sw^{-/-}$) so that the LVAVA and LIAVA variants could be investigated in isolation of the mouse S pigment, which normally is coexpressed with the M/L pigment in a subset of mouse cones.[29–31] The double mutant lines studied here were: $Opn1lw^{LIAIS}$ $Opn1sw^{-/-}$, $Opn1lw^{LVAVA}$ $Opn1sw^{-/-}$, and $Opn1lw^{LIAVA}$ $Opn1sw^{-/-}$. All mice used in experiments described here were verified by genotyping using the polymerase chain reaction as previously described in detail.[27] The $Opn1sw^{-/-}$ and $Opn1lw^{LIAIS}$ $Opn1sw^{-/-}$ lines were previously described and validated.[27] Males and females were used interchangeably in this study.

Electroretinogram (ERG)

Cone photoreceptor function was examined using the On-Off (long-flash) ERG with L/M cone isolating stimuli or with S cone isolating stimuli generated using silent substitution. Humans and mice were light adapted under standard fluorescent room lighting, and ERGs were performed under photopic conditions with background light levels adjusted to favor cone responses over rods. The methods and apparatus for obtaining L/M and S cone ERGs were reported previously for mice[27] and humans.[32] In the photopic ERG, the a-wave is considered to be generated by a combination of cones and OFF-bipolar cells, while b- and d-waves are considered to reflect primarily ON-bipolar and OFF-bipolar cell activity, respectively.[33]

Each ERG trace was the averaged data obtained from a defined number of stimulus presentations. For all mice and humans with "normal" L/M cone opsins, the number of presentations was set to 20. For humans with mutant L/M opsins, the number of stimulus presentations was 50 to 100.

The ERG apparatus used a built-in system that automatically rejected traces exceeding a certain value to ensure that responses contaminated by blink or movement artifacts were not included in the final average. Multiple averaged traces were recorded for each subject and the standard error of the mean was calculated for the mean of the averaged traces to give an indication of reliability.

Immunocytochemistry and Image Acquisition in Mice

Mice were euthanized with a lethal dose of sodium pentobarbital. For comparisons of $Opn1lw^{LIAIS}$ $Opn1sw^{-/-}$, $Opn1lw^{LVAVA}$ $Opn1sw^{-/-}$, and $Opn1lw^{LIAVA}$ $Opn1sw^{-/-}$ mice, time points were ages 3 months (4 per line) and 16 months (5 per line). Tissue was fixed via intracardial perfusion of 4% paraformaldehyde followed by a mixture of 4% paraformaldehyde plus 1% glutaraldehyde. Eyes were dissected and 100 μm thick sagittal sections were cut with a vibratome so that each section contained dorsal and ventral retina. Sections were incubated with 1% sodium borohydride in PBS for 30 minutes at room temperature (RT), washed in PBS, then incubated overnight at 4°C in a solution of 5% donkey serum (Cat #017-000-121; Jackson ImmunoResearch, West Grove, PA), 1 mg/ml BSA (Cat #001-000-161; Jackson ImmunoResearch), and 0.03% Triton X-100 in PBS (pH 7.4). Primary antibodies were rabbit anti-M/L-opsin (Cat #AB405; Merck Millipore, Billerica, MA) diluted 1:200 and goat anti-S-opsin (Cat #sc-14365, Santa Cruz Biotechnology, Dallas, TX) diluted 1:100. Primary antibodies were incubated at 4°C for at least 3 days for sections and 2 days for whole mount tissue. Specimens were washed in PBS three times for 30 minutes each and incubated overnight at 4°C with 4′,6-diamidino-2-phenylindole (DAPI), dihydrochloride (1:10,000; Cat #D-21490; Invitrogen,

Carlsbad, CA), fluorescein-conjugated PNA (Cat #FL-1071; Vector Laboratories, Inc., Burlingame, CA), and secondary antibodies. Secondary antibodies were Alexa Fluor 555 labeled donkey anti-rabbit IgG (H+L) diluted 1:200 (Cat #A31572, Invitrogen) in antibody dilution buffer and Alexa Fluor 633 labeled donkey anti-goat IgG (H+L) diluted 1:200 (Cat #A21082; Invitrogen). This was followed by three 30-minute PBS washes, 30 minutes of post-fixation with 4% paraformaldehyde, and three more 30-minute PBS washes. Finally, sections were placed on slides with 2% 1,4-diazabicyclo(2.2.2)octane (DABCO) in glycerol and cover-slipped. Nuclei and cone sheaths were labeled with DAPI and PNA, respectively.

Retinal images were acquired using wide-field microscopy at ×30 magnification. All images, 292.5 μm in width, were taken approximately 200 μm from the ora serrata within the dorsal region of sagittal vibratome sections that had been immunolabeled for L-opsin. Fifty optical sections were taken for each specimen at 0.5-μm intervals. The Z-stack was reconstructed in Image J (available in the public domain at https://imagej.nih.gov/ij/) and oriented so that the lengths of the outer segments were in plane. Individual cone outer segment lengths, identified by the *L* opsin labeling, were measured in a 5.7 mm^2 × 19.5 μm deep volume and then counted in a 2.8 mm^2 × 9.5 μm deep subvolume. The unpaired *t*-test was used to determine whether differences observed between mouse lines were statistically significant.

Confocal images were acquired using an Olympus (Tokyo, Japan) FluoViewTM FV1000 confocal microscope with a ×60 oil-immersion lens. Z-stacks were combined using Image J software,[34] and channel exposure levels were balanced within and across images using Adobe Photoshop as previously described.[27]

Minigene Assays

We created minigene constructs in the pFLAG-CMV-5a vector using the procedures described in detail by Ueyama et al.[15] Briefly, we replaced the *Bbs*I fragment extending from exon 2 to exon 4 of a human *L* opsin cDNA with the corresponding fragment from genomic DNA from subject 10-0059 (*LVAVA*), subject 11-0271 (*LIAVA*), and from a subject with the *LVAIS* variant. The haplotypes for these individuals in terms of the nucleotides at exon 3 cDNA positions 513, 517, 525, 571, 573, 581, 592, and 598 are GCGGGCGG for *LVAVA*, GCGATCGG for *LIAVA*, and GCGGGCAT for *LVAIS*. We also made minigenes from subjects with *MIAVA* (nucleotide haplotype AACATCGG) and *LVVVA* (nucleotide haplotype GCGGGGGG). The *MIAVA* and *LVVVA* variants were associated previously with vision disorders[14,17] and shown to cause aberrant splicing.[15,17] We made the *LIVVA* (GCGATTGG) variant, which has not been reported in a human patient, by site directed mutagenesis. The opsin cDNA we used matched the sequence of the hs7 opsin cDNA originally described by Nathans et al.[28] The exon 2 haplotype was CAAC at c.DNA positions 194, 300, 331, and 347, respectively, and the exon 4 haplotype was TGCTA for c.DNA positions 689, 697, 698, 699, and 706. Plasmids containing the minigenes were isolated using the Qiagen Miniprep kit (Qiagen, Hilden, Germany), and sequence verified using the BigDye Terminator v3.1 Cycle Sequencing Kit (Applied Biosystems, Foster City, CA) and the ABI Prism 3500 Genetic Analyzer (Applied Biosystems).

Two independent minigene clones were used to transiently transfect HEK293T cells (American Type Culture Collection, Manassas, VA) using FuGene HD (Promega, Madison, WI). Cells were cultured in Dulbecco's modified Eagle's Medium (Gibco Laboratories, Gaithersburg, MD) containing 10% HyClone Cosmic Calf serum (Thermo Fisher Scientific, Waltham, MA). Duplicate wells of HEK293T cells were transfected with each of the minigene clones and incubated for 2 days. Total RNA was isolated from the cells using the Qiagen RNeasy Kit (Qiagen). Messenger RNA was converted to cDNA using reverse transcriptase followed by the polymerase chain reaction (RT-PCR). RNA (1 μg) from each sample was used with the Superscript First Strand Synthesis System (Invitrogen) primed with Oligo(dT) following the manufacturer's recommendations. Two μl of the RT reaction were used for PCR with a forward primer corresponding to codons 59 through 65 in exon 2 (5′-TGGATGATCTTTGTGGTCA-3′) and a reverse primer to the flag tag sequence (5′-CTTGTCATCGTCGTCCTTGTA-3′). The PCR conditions were 94°C for 2 minutes and then 25 cycles of 94°C for 30 seconds, 55°C for 30 seconds and 72°C for 1 minute, with a final extension at 72°C for 2 minutes. The PCR product was analyzed by agarose gel electrophoresis using the Quickload 100bp Ladder (New England Biolabs, Inc., Ipswich, MA) as molecular weight markers. DNA bands were extracted from the gel and directly sequenced. We also isolated individual bands from the gel, and following a purification step, ligated the DNA into plasmid pCMV5α and sequenced 5 individual clones.

Table 1. Summary of Subject Characteristics

Subject	Age	Axial Length OD,OS	Spherical Equivalent Refraction in Diopters OD,OS	BCVA OD,OS	*L/M* Array Structure[a]	Color Vision Testing Results Summary
10-0059[b]	33y	24.77, 24.25	−3.3, −2.0	20/200, 20/150	L^{LVAVA} (1L, 0M)	deuteranope, cone dystrophy
11-0115[c]	45y	27.08, 26.58	−5.8, −4.9	20/100, 20/150	M^{LVAVA} (0L, 1M)	protanope, cone dystrophy
11-0271[e]	32y	30.91, 31.18	−15.25, ND[d]	20/200, 20/200	L^{LIAVA} M^{MVVVA} (1L, 1M), *L* promoter -3T>C	incomplete achromatopsia with residual *M* cone function

[a] Top row is the opsin gene variant, second row is the estimate number of *L* and *M* genes per array. Single letter amino acid code: L, leucine; I, isoleucine; A, alanine; V, Valine; M, methionine.
[b] Subject JC_0347.[14]
[c] Subject JC_0564.[14]
[d] ND, not done.
[e] Subject MF.[11]

Bioinformatics Analysis of Exon 3 Variants Using Human Splicing Finder 3.0

The computer program Human Splicing Finder (HSF)[35] was used to identify motifs that act as ESEs, ESSs, exon identity elements (EIE), intron identity elements (IIE), and exonic splicing regulators (ESR) that included one or more nucleotides at the polymorphic positions within exon 3. The positions were, in terms of cDNA nucleotide numbers, 453 (codon 151), 457 (codon 153), 465 (codon 155), 511 and 513 (codon 171), 521 (codon 174), 532 (codon 178), and 538 (codon 180). Motifs were identified by one of two methods. Some motifs, such as the ESE SRp40, ESE SC35, ESS hnRNPA1, ESS Sironi Motif, 9G8 ESE, and ESE FS2/ASF, were identified based on a consensus sequence value relative to a defined threshold value. If a sequence exceeded the threshold, the motif was identified. The second method used to identify motifs such as FAS, ESS, ESR, IIE, EIE, and PESE was based on comparison to various databases of motifs.

Results

Genotype and Phenotype of Subjects

We examined two subjects with an *LVAVA* opsin gene variant and one with an *LIAVA* variant. All three subjects had participated in other studies.[11,14] Table 1 summarizes characteristics of each subject as measured in this study. For subject 10-0059, the MassArray assay and direct sequencing showed that he had a single cone opsin gene on his X-chromosome, and it was an *L* opsin gene that specified the *LVAVA* variant. For subject 11-0115, the MassArray data and sequencing also indicated a single cone opsin gene on the X-chromosome; it was an *M* opsin gene that specified the *LVAVA* variant. These findings are in agreement with a previous report.[14] Here, we also sequenced the exons and intron/exon junctions of the *S* opsin genes for both subjects and found that the sequences matched the reference sequence in the December 2013 assembly of the human genome (GRCh38/hg38).

For subject 11-0271, the MassArray and sequencing data indicated that he had a single *L* opsin gene that encoded the *LIAVA* variant, and a single, normal *M* opsin variant. This finding is not in agreement with a previous report for the number of *L* and *M* opsin genes for this subject estimated using a custom TaqMan assay that has been described in detail.[11,36] To reconcile the difference between the TaqMan versus MassArray estimates, we sequenced the promoter region of 11-0271's *OPN1LW* and *OPN1MW* genes, including the region to which the primers, probes and extension primers in the TaqMan and MassArray assays bind. In the promoters of both genes, there is a C residue at the −3 position (where the mRNA start

site is +1). Normally the *L* gene has a T residue at the −3 position and the *M* gene has a C residue.[28] None of the oligonucleotides used in the MassArray assay bind to the −3 position; however, the TaqMan probes for estimating the number of X-chromosome opsin genes does bind to the −3 position. Having a C at the −3 position in all X-chromosome opsin genes leads to an overestimate of the total number of genes. Thus, the MassArray data provide a more accurate estimate of the number of X-chromosome opsin genes for this subject. Sequencing confirmed that 11-0271's *OPN1LW* gene specifies the *LIAVA* variant, his *OPN1MW* gene is normal, and the sequences are in agreement with those found previously.[11]

The best corrected visual acuities for all three subjects were measured in this study, as were the axial lengths and corneal curvature. The latter two metrics were used to calculate the spherical equivalent refraction, with differences from previously reported values being within the error of the measurement.[11,14] For each subject, these measurements and the color vision tests results are summarized in Table 1.

Functional Analysis of *L/M* and S Cones in Males with a Single X-Chromosome Cone Opsin Gene Specifying the *LIAVA* or *LVAVA* Variant

Full field S and L/M cone-isolating On-Off ERGs were performed on the subjects with *LVAVA* and *LIAVA* opsin variants. Five males with normal color vision served as control subjects, and sequencing verified that each of them had *OPN1LW* and *OPN1MW* genes associated with normal vision. The mean age for the control group was 27 years with a range from 22 to 33 years.

Full field On-Off ERGs were recorded in response to L/M or S cone-isolating stimuli for subject 11-0271 with the $OPN1LW^{LIAVA}$ gene (Fig. 1). Under L/M cone isolating conditions, there was no detectable retinal response to full-field stimulation by 525 nm or 641 nm light in 11-0271 (Fig. 1A), whereas the control subjects all showed the typical L/M cone ERG waveform (Fig. 1A). Under S cone isolating conditions, subject 11-0271 yielded a typical S cone ERG with characteristic a- and b-waves (Fig. 1B). There was no d-wave observed with the S cone isolating stimulus, presumably because there is no S cone–specific OFF bipolar cell.[37] Approximately 6% of the cone photoreceptors in normal human retina are S cones,[38] the remaining 94% are L and M cones. Thus, the S cone ERG a- and b- wave amplitudes are expected to be

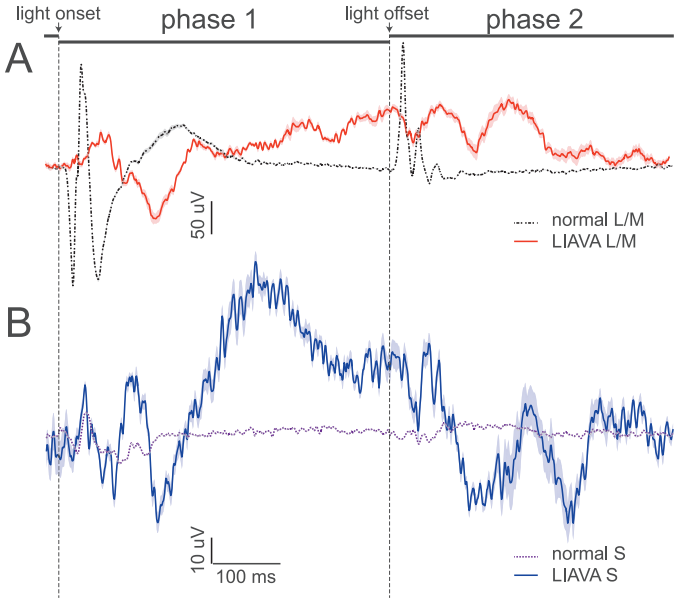

Figure 1. Full field, On-Off ERGs for $OPN1LW^{LIAVA}$ subject 11-0271 compared to control subjects with normal vision (A). The L/M response for control subjects is shown in *black*, and the response for the subject with the $OPN1LW^{LIAVA}$ opsin gene variant is shown in *red*. The response of the control subjects represents the average of traces from 7 subjects, each trace represents the average response from a minimum of 20 stimulus presentations. The L/M cone response shown for the subject with the $OPN1LW^{LIAVA}$ opsin gene variant (*red trace*) is the average of 6 traces from one subject, with each trace representing the average of 50 to 100 stimulus presentations. The shading for the red trace shows the standard error of the mean for each data point. Characteristic features of the normal ERG that occur at light onset and light offset (a, b, and d-waves are labeled) were not detected in this subject, indicating an absence of *L/M* cone function. Note, stereotyped ocular muscle movements associated with photophobia for the *LIAVA* subject produce characteristic responses in the ERG that are time-locked to the onset and offset of light. These responses are neither discarded by thresholding to reject blinks and other artifacts nor are they nulled by averaging. The small standard error of the mean demonstrates the ERGs from the $OPN1LW^{LIAVA}$ subject are highly reliable and accurately reflect the loss of normal cone photoreceptor and bipolar cell function in this subject. (B) ERGs in response to an *S* cone-isolating stimulus. The average of 48 traces, with each trace representing the average of at least 20 stimulus presentations from control subjects is shown in *black*. In *blue* is the average of 7 traces, with each trace representing the average of 50 to 100 stimulus presentations for subject 11-0271 with the $OPN1LW^{LIAVA}$ opsin gene. The shading for the ERG response shown in *blue* gives the standard error of the mean for each data point. The *S*-cone response for the subject with $OPN1LW^{LIAVA}$ opsin gene included a strong response at light onset that was consistent with that of a normal ERG S-cone cone generated B-wave in temporal profile with a slightly higher amplitude than normal.

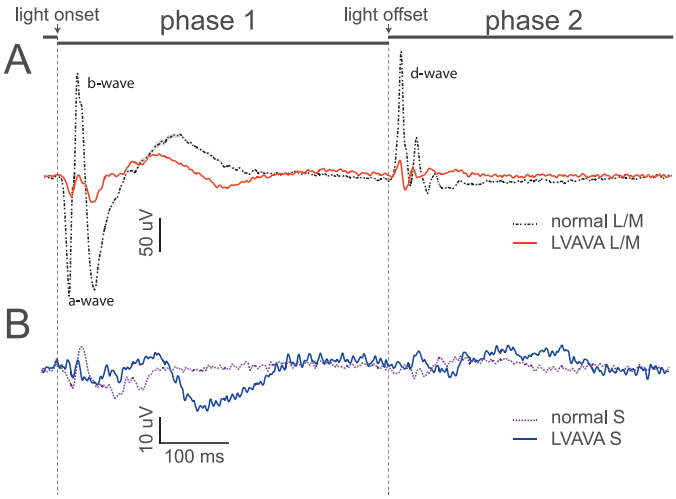

Figure 2. Full field, On-Off ERGs for *OPN1LW*^{LVAVA} subjects 10-0059 and 11-0115. (A) The average *L/M* cone-isolated ERG recorded from 7 control subjects is shown in *black*, and is the same as in Figure 1A. The characteristic a-, b- and d- waves are indicated. The *red line* shows the average from 2 subjects with an *OPN1LW*^{LVAVA} variant, with each trace being the average of 50-100 stimulus presentations. (B) Shown are the averages of full-field ERGs in response to an *S* cone isolating stimulus for 7 control subjects, and the averages for the two subjects with *LVAVA* opsin variants. For the *OPN1LW*^{LVAVA} subjects, retinal responses to *S*-cone-isolating stimuli with the timing of b-waves were not above the noise. These results indicate that *S*-cone responses are low or nonexistent compared to normal suggesting that the *OPN1LW*^{LVAVA} gene conveys toxicity to neighboring S cone photoreceptors.

relatively small compared to amplitudes from *L/M* cone ERGs.

Subjects 10-0059 with an *OPN1MW*^{LVAVA} gene and 11-0115 with an *OPN1LW*^{LVAVA} gene both showed clear, but diminished a-, b- and d- waves under *L/M* cone isolating conditions compared to the normal controls (Fig. 2A). For example, in response to a 525 nm light stimulus, the average b-wave amplitude from these two subjects was 88.4% lower than the average of the five control subjects ($P < 0.01$). However, compared to the typical *S* cone ERG waveform of control subjects, the retinal response under *S* cone isolating stimuli for the two subjects with *LVAVA* opsin genes was not above the noise (Fig. 2B). The signal-to-noise ratio for S-cone ERGs is small because of the small fraction of *S*-cones in the normal retina. Nonetheless, the difference in the *S*-cone response between the *LVAVA* subjects and the normal subjects (Fig. 2B) still is quite clear and we concluded that no significant S-cone ERG is recordable in the subjects with the *LVAVA* opsin genes.

Table 2. ERG Time Course in *LIAIS* Versus *LIAVA* Mice

Mouse Line[a]	Age, Mos.	No. Mice	B-Wave, μv	SEM[b]	*P* Value
LIAIS	1.5	10	131.4	15.1	0.39
LIAVA	1.5	10	151.2	11.4	
LIAIS	3	10	99.3	9.3	0.39
LIAVA	3	10	118.5	13.2	
LIAIS	6	7	86.4	12.7	0.7
LIAVA	6	10	82.7	7.4	
LIAIS	9	10	98.7	6.8	0.81
LIAVA	9	10	96.2	8.5	
LIAIS	12	10	90.0	9.2	0.061
LIAVA	12	10	66.6	8.2	
LIAIS	16	10	70.7	5.8	0.021
LIAVA	16	7	49.7	6.2	

[a] LIAIS mice are *Opn1lw*^{LIAIS} *Opn1sw*$^{-/-}$; *LIAVA* mice are *Opn1lw*^{LIAVA} *Opn1sw*$^{-/-}$.
[b] SEM, standard error of the mean.

All three subjects with an *L/M* interchange mutant opsin had nystagmus, although it was less severe for the *LVAVA* subjects than for the *LIAVA* subject. All three were photophobic, and as a consequence, each made small but highly reliable movements of orbital muscles that produced electrical responses that were time-locked to the light stimulus, and, thus, were evident in the ERG recordings, but they do not reflect retinal responses. For example, in Figure 1A, the ERG response of the *LIAVA* subject to the L/M isolating stimulus does not show any normal a- or b-wave, but there is a slower hyperpolarization followed by a depolarization, which starts just after the b-wave in the normal response. Similarly, the *LIAVA* subject does not show any normal d-wave, but there are slower components that we attribute to these small involuntary ocular muscle movements that occur with each stimulus presentation. The shaded area around the trace shows the standard error of the mean calculated from a series of averages demonstrating that the ERG traces are highly reliable, and thus, accurately reflect the absence of cone photoreceptor and bipolar cell responses in the subjects.

Cone Function in Double Mutant Mice with *Opn1lw*^{LIAVA} *Opn1sw*$^{-/-}$, or *Opn1lw*^{LVAVA} *Opn1sw*$^{-/-}$ Compared to Control Mice with *Opn1lw*^{LIAIS} *Opn1sw*$^{-/-}$

We performed L/M-isolating On-Off cone ERGs in *Opn1lw*^{LIAVA} *Opn1sw*$^{-/-}$, and *Opn1lw*^{LIAIS}

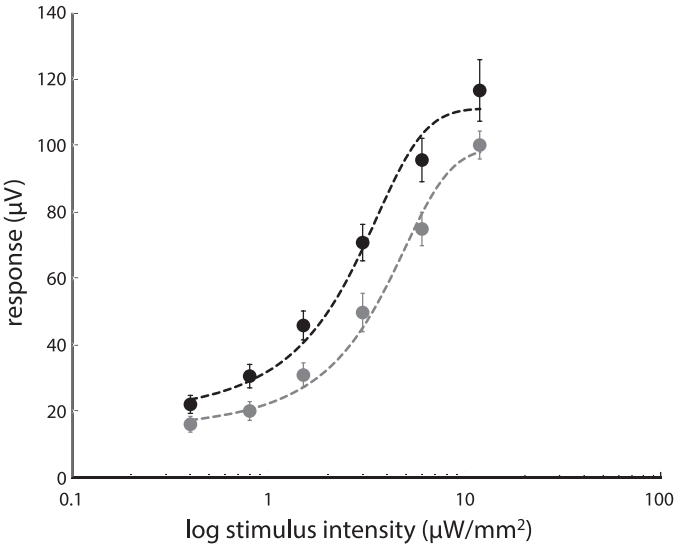

Figure 3. Intensity response functions for *Opn1lw*^{LIAVA} *Opn1sw*$^{-/-}$ versus *Opn1lw*^{LIAIS} *Opn1sw*$^{-/-}$ mice. Full-field, On-Off ERGs to an LM cone isolating stimulus in a light intensity series ranging from 0.4 to 11.8 μW/mm^2 were measured in 16-month-old *Opn1lw*^{LIAIS} (*black symbols*, $n = 10$) and *Opn1lw*^{LIAVA} (*gray symbols*, $n = 7$) mice. Data were fit with a cumulative normal function. *Error bars*: SEM. The only age at which a significant difference was observed between the *LIAIS* and *LIAVA* mice was 16 months.

Opn1sw$^{-/-}$ mice, and the results are summarized in Table 2. Retinal responses as a function of age were measured in the same mice at 3, 6, 9, 12, and 16 months of age, and in a separate set of mice at 1.5 months using a 3.0 μW/mm^2 light stimulus. An age-dependent decrease in ERG amplitude was observed in both lines, consistent with what has been reported previously for wild type C57Bl/6 mice[39] and for *Opn1lw*^{LIAIS} *Opn1sw*$^{-/-}$ control mice.[27] Only at the 16-month time point was there a significant difference between the LIAIS versus *LIAVA* mice, when the b-wave amplitudes were reduced by 29.7% ($P < 0.05$) for the *Opn1lw*^{LIAVA} *Opn1sw*$^{-/-}$ mice ($n = 7$), compared to the *Opn1lw*^{LIAIS} *Opn1sw*$^{-/-}$ mice ($n = 10$). This result is illustrated in Figure 3, which shows that 16-month-old *Opn1lw*^{LIAVA} *Opn1sw*$^{-/-}$ mice gave consistently lower responses than the *Opn1lw*^{LIAIS} *Opn1sw*$^{-/-}$ mice for light intensities ranging from 0.4 to 11.8 μW/mm^2.

In contrast, the *Opn1lw*^{LVAVA} *Opn1sw*$^{-/-}$ mice had significantly reduced *L* cone responses compared to the *Opn1lw*^{LIAIS} *Opn1sw*$^{-/-}$ mice at all of the time points tested under *L*/*M* cone isolating conditions (Fig. 4A). On average, the b-wave amplitudes in the *Opn1lw*^{LVAVA} *Opn1sw*$^{-/-}$ mice were 24.6 μV ± 4.0 lower than in the *Opn1lw*^{LIAIS} *Opn1sw*$^{-/-}$ control

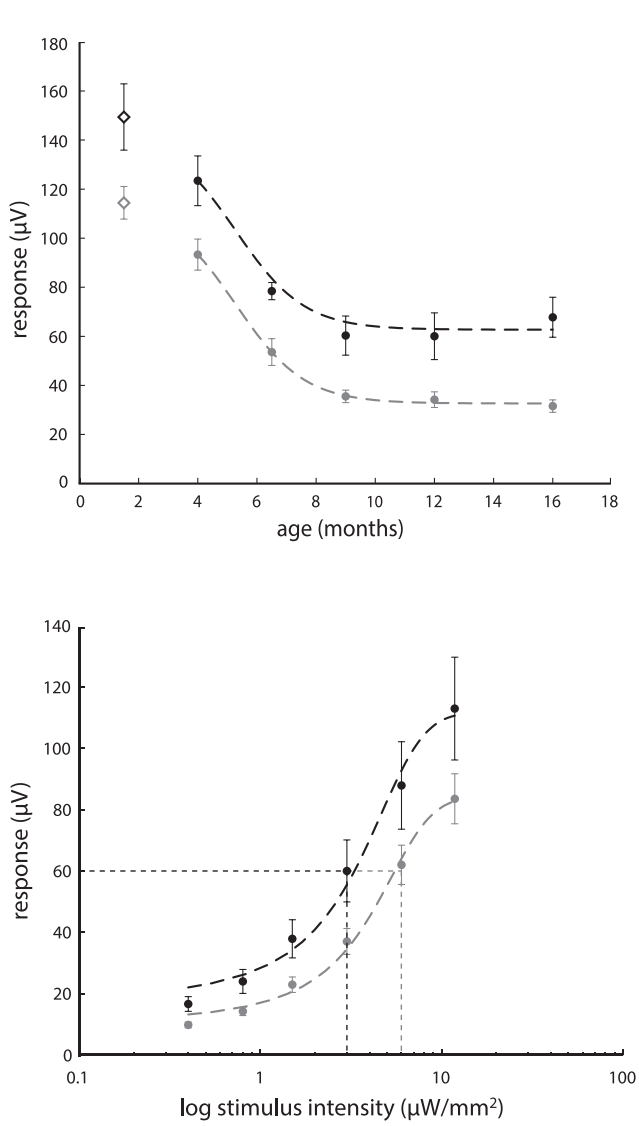

Figure 4. ON-OFF ERGs in *Opn1lw*^{LVAVA} *Opn1sw*$^{-/-}$ versus *Opn1lw*^{LIAIS} *Opn1sw*$^{-/-}$ mice. *L* cone ERGs were collected from *Opn1lw*^{LIAIS} (*black symbols*) and *Opn1lw*^{LVAVA} (*gray symbols*) across 16 months. (A) Using a 520 nm light stimulus (3.0 μW/mm^2), retinal responses were measured in the same mice from 4 months through 16 months of age (*circles*) and in a separate set of mice at 6 weeks of age (*diamonds*). The *Opn1lw*^{LVAVA} mice (*gray circles* and *dashed lines*) had significantly weaker responses at each time point compared to the *Opn1lw*^{LIAIS} mice. (B) Retinal responses to an intensity series ranging from 0.4 to 11.8 μW/mm^2 are shown for the mice at 12 months of age. The *Opn1lw*^{LVAVA} mice (*gray circles*) had weaker responses at each time point compared to *Opn1lw*^{LIAIS} mice (*black circles*). The *dotted lines* illustrate that approximately twice the light intensity would be needed to generate a 60 μV ERG from the *Opn1lw*^{LVAVA} mice as from the *Opn1lw*^{LIAIS} mice. Data were fit using a cumulative normal function (*dashed traces*). *Error bars*: SEM.

mice, and the reduction was observed across a broad range of light levels (Fig. 4B). The dotted lines in Figure 4B illustrate that approximately twice as much light is required to generate a 60 μV ERG in the *Opn1lw*^{LVAVA} *Opn1sw*$^{-/-}$ mice versus in the *Opn1lw*^{LIAIS} *Opn1sw*$^{-/-}$ control mice.

Effects of *Opn1lw*^{LIAVA} and *Opn1lw*^{LVAVA} Photopigments on Cone Outer Segment Number and Length in S-Opsin Knockout Mice

To evaluate the structural integrity of the *LIAVA* and *LVAVA* cones, outer segments were counted and measured in length in dorsal retina. Outer segment numbers and lengths were not significantly different for 3-month-old ($n = 4$ mice per line) or 16-month-old ($n = 5$ mice per line) *Opn1lw*^{LIAVA} *Opn1sw*$^{-/-}$ versus the *Opn1lw*^{LIAIS} *Opn1sw*$^{-/-}$ control mice. In contrast, the lengths of the *Opn1lw*^{LVAVA} *Opn1sw*$^{-/-}$ cone outer segments in the dorsal retina were 16.1% shorter ($P < 0.03$) at 3 months of age and 23.2% shorter ($P = 0.02$) at 16 months compared to the *Opn1lw*^{LIAIS} *Opn1sw*$^{-/-}$ control mice; however, there was no significant difference between the two lines of mice in the numbers of cone outer segments at either age (data not shown). Confocal microscopy and immunohistochemistry with an anti-L/M opsin antibody showed that there was much less cone opsin in the outer segments of the *LVAVA* mice compared to the *LIAVA* and *LIAIS* mice at 3 months of age, and there also was less *L/M* opsin in the *LVAVA* compared to *LIAIS* mice at 16 months of age, as illustrated in Figure 5.

Splicing Products Observed for Minigenes that Differed Only in the Sequence of Exon 3

The RT-PCR products from the splicing assay were visualized by agarose gel electrophoresis and the bands observed (Fig. 6) were gel purified and sequenced either directly or after subcloning. For the control *LVAIS* variant, there was only one major band, labeled "e," and its sequence was that of the full-length *LVAIS* variant. For each of the *LIAVA*, *MIAVA*, *LIVVA*, *LVAVA*, *LIAVS*, and *LVVVA* variants, there was a prominent band, labeled "c" and for each variant, the sequence of this band shows that exon 2 was spliced directly to exon 4 and that exon 3 was absent. For the *LIAVS* and *LVVVA* variants, the most prominent band ran with a slightly larger apparent molecular weight than the full-length band observed for the *LVAIS* control, and is labeled "b." A band running at this molecular weight also was observed for the *LIAVA*, *MIAVA*, *LIVVA*, and *LVAVA* variants, although it was much fainter than the corresponding band for the *LIAVS* and *LVVVA* variants. Sequencing of this band for each variant revealed that a mixture of correctly spliced full-length product and exon 3 skipped product. Presumably, these two products form heteroduplexes. Secondary structure in mismatched regions of heteroduplexes, in this case the single strand region containing exon 3, slows the migration rate of the heteroduplexes through the gel, hence heteroduplexes migrate at a rate not predicted strictly by their molecular weight. Two additional bands, labeled "a" and "d" were observed for all variants including the control, if enough PCR product was loaded on the gel. The band labeled "a" was shown by sequencing to have correctly spliced out intron 2 but retained the 3′ most 425 bases of intron 3, while the band labeled "d" contained exon 2 spliced to exon 6. Given that these latter two PCR products were observed for the control, as well as the other variants, they may represent either a normal level of missplicing or an artifact of the minigene assay, but in either case they are unlikely to contribute to the deleterious vision phenotypes associated with the *L/M* interchange mutants.

Map of Exonic Splicing Regulators

Figure 7 shows a map of the ESE and ESS motifs identified by the algorithms available in HSF 3.0 for the exon 3 variants investigated in the minigene assay. ESEs promote exon inclusion and ESSs promote exon exclusion from the mRNA. HSF also identifies motifs for ESR that can function as enhancers or silencers of splicing depending on the context, EIEs that are important for exon recognition, and IIEs that are important for intron recognition.[40] IIE motifs in an exon may promote exon exclusion and would, thus, be categorized as ESS. In the context of the *L/M* opsin gene exon 3, the ESR and EIE motifs are categorized as ESEs and the IIE motifs are categorized as ESSs. The results shown in Figure 7 show that motifs for ESEs, but not for silencers, are found in the region encoding codons 168 through 183 of the *LIAIS* variant. Thus, changing codon 178 from ATC to GTC and changing codon 180 from TCT to GCT destroys enhancers and creates silencers.

Figure 7 also shows that when codon 171 is ATT there are overlapping binding motifs for two SR proteins, SC35 and SRp40. SR proteins are trans-splicing factors and are so named due to the presence

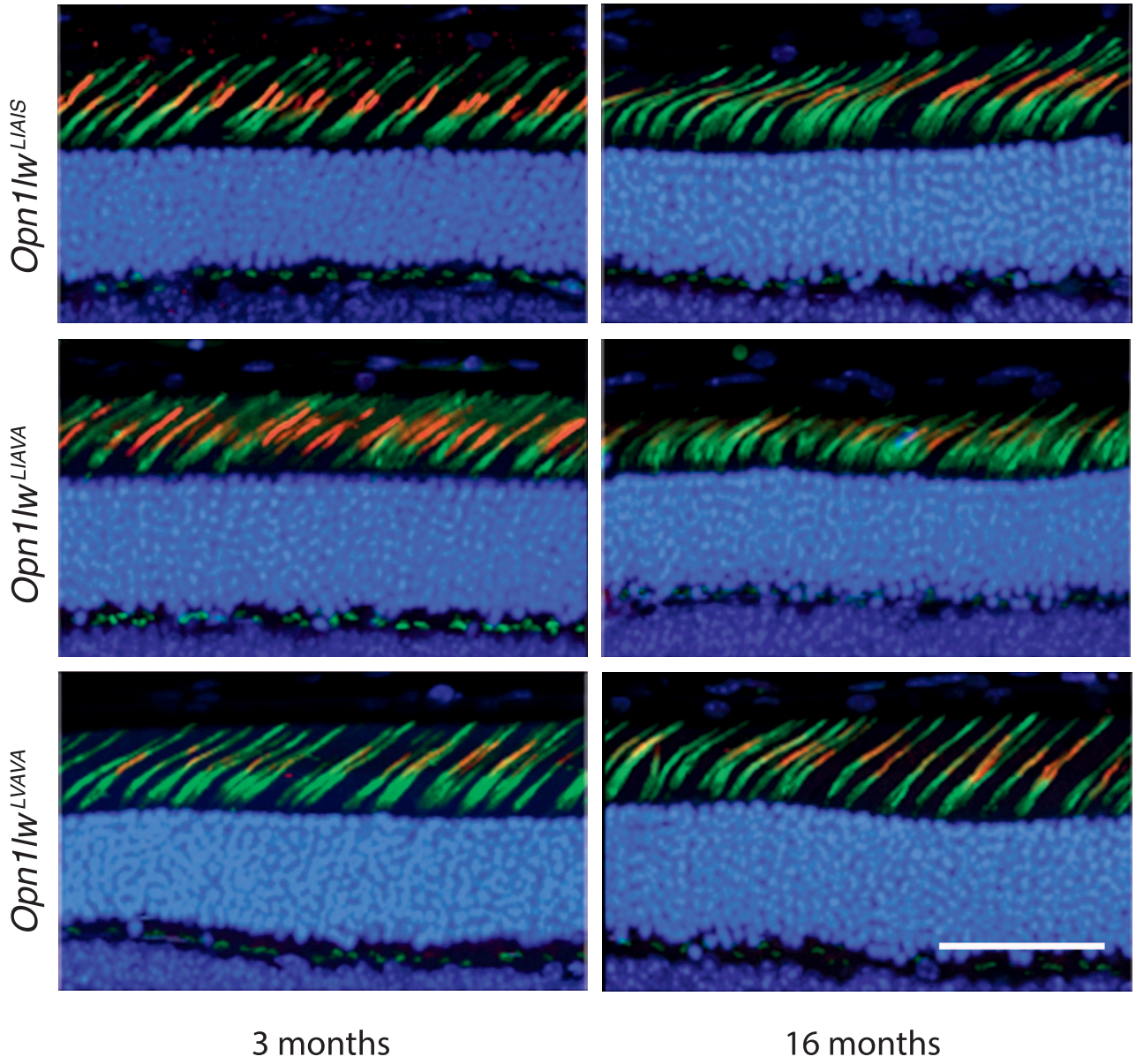

Figure 5. Immunohistochemical analysis of cone outer segment morphology in *Opn1lw*^{LIAIS}, *Opn1lw*^{LIAVA} and *Opn1lw*^{LVAVA} mice. Confocal images were acquired using an Olympus FluoViewTM FV1000 confocal microscope with a ×60 oil-immersion lens. Z-stacks were combined using Image J software[34] and channel exposure levels were balanced within and across images using Adobe Photoshop as previously described.[27] Confocal images of sagittal, vibratome sections were acquired at the far dorsal retina in mice that were sacrificed at 3 months (*left column*) and 16 months (*right column*) of age. *M*-opsin (*red*), cone sheaths (*green*/PNA), and nucleic acid (*blue*/DAPI) were labeled, and representative images are shown. 20 μm z-stacks (0.5 μm spacing) were imaged at ×60 magnification. *Scale bar*: 33.3 μm.

of domains with long repeats of serine (S) and arginine (R) residues. The consensus value threshold for SC35 binding motifs defined by HSF is 75.05. The consensus value score for the SC35 motif is slightly greater when codon 171 is GTG (82.61) compared to when it is ATT (79.84). Furthermore, when codon 171 is ATT, there is an SRp40 binding motif with consensus value score of 84.25, which is above the defined threshold of 78.08. When codon 171 is changed to GTG, the SRp40 binding motif is broken because the consensus value score falls below the threshold. Finally, when codon 171 is ATT, an ESR motif is identified as having enhancer function that is absent when the codon is GTG.

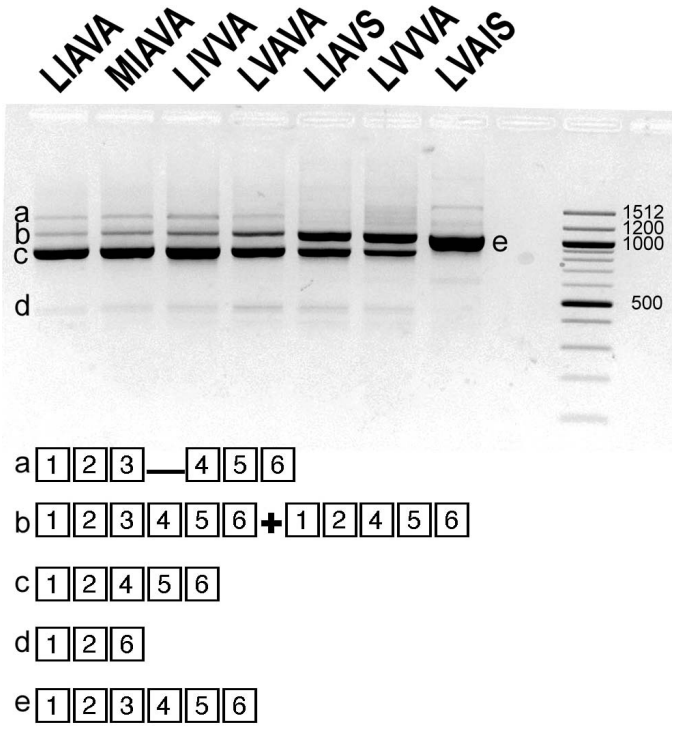

Figure 6. Agarose gel (1.5%) showing RT-PCR products from the minigene splicing assay. The exon 3 variant is indicated above each lane. The *far right* lane contains molecular weight markers (Quickload, 100 bp ladder, New England Biolabs), and the sizes in base pairs are indicated for a subset of them. The bands labeled with letters "a", "b" and "d" indicate bands that were present in all variants including the *LVAIS* control. Band "c" was found in all of the variants except the *LVAIS* control, and band "e" was found only in the *LVAIS* control. Below the gel is a schematic (not to scale) of the contents of each band, with exons indicated by *boxes*, and retained intron sequences indicated by a *black line*. Band "a" contained all exons plus 425 bp from the 3′ end of intron 3. Band "b" contained a mixture of exon 3-skipped and full-length product, presumably in the form of heteroduplexes for which secondary structure in single stranded regions accounts for why this band runs at a higher molecular weight than full-length (band "e") or exon 3 skipped alone (band "c"). Band "c" contains exon 3 skipped mRNA, with exon 2 spliced to exon 4. Band "d" contains exons 1, 2, and 6. Band "e" contained only the full-length cDNA product. The gel image was imported into Adobe Photoshop, inverted, and the contrast enhanced for easy viewing of bands that were faint in the original image.

Discussion

Human *LIAVA* Cone Phenotype Attributable Entirely to the Splicing Defect

The results reported here are consistent with the conclusion that subject 11-0271 has a negligible number of functional *M* cones, if any. Although he has a normal *M* opsin gene, the promoter of his *L* gene has a mutation at the −3 position that is associated with an extremely high ratio of *L* to *M* cones.[23,38] No *M* cone function was detected previously with the flicker photometric ERG[11] nor was it detected with the *L*/*M* cone-isolating On-Off ERG used in this study, although previous psychophysical data suggested he might have some residual *M* cone function.[11] The only major RT-PCR product detected in the assay using a minigene derived from this subject's $OPN1LW^{LIAVA}$ gene lacked exon 3 and had exon 2 spliced directly to exon 4, introducing a frame shift and a premature translation termination codon seven codons past the exon 2/exon 4 splice junction. This mRNA is very likely targeted for degradation in the nonsense-mediated decay pathway,[41,42] and this can account for the absence of *L* cone function in this subject. *S* cone function appears to be unaffected by the *L* cones that lack photopigment.

It was not possible to use adaptive optics imaging to visualize the cone mosaic in subject 11-0271 due to his severe nystagmus. However, retinas with normal *S* and *M* cones, and cones that presumably transcribe an $OPN1LW^{LIAVA}$ opsin gene and retinas with normal *S* and *L* cones and cones that presumably transcribe an $OPN1MW^{LIAVA}$ opsin gene have been imaged with adaptive optics[10,18] and show that the cones that presumably transcribe the *LIAVA* opsin gene appear to be intact and viable, but do not contain any photopigment as evidenced by the complete absence of wave guiding by the outer segment. These results supported the conclusion that the *LIAVA* variant opsin gene haplotype causes a splicing defect that results in the absence of cone function and that vision disorders observed in humans with the *LIAVA* variant can be attributed entirely to the splicing defect, which appears to be complete. The observation that the *LIAVA* photopigment functions normally in mice, with no deleterious consequences on cone photoreceptors beyond what is observed as part of normal aging in mice[27] suggests that there is no defect in the *LIAVA* opsin at the level of protein structure and function, further supporting the conclusion that the cone phenotype in human subjects is entirely attributable to misplicing of the *LIAVA* opsin pre-mRNA. Previous adaptive optics and optical coherence tomography imaging of patients with an *LIAVA* opsin gene suggest that the cone defect is stationary.[14] Thus, it seems likely that these cones could be made functional using gene therapy. Significant improvement in visual acuity

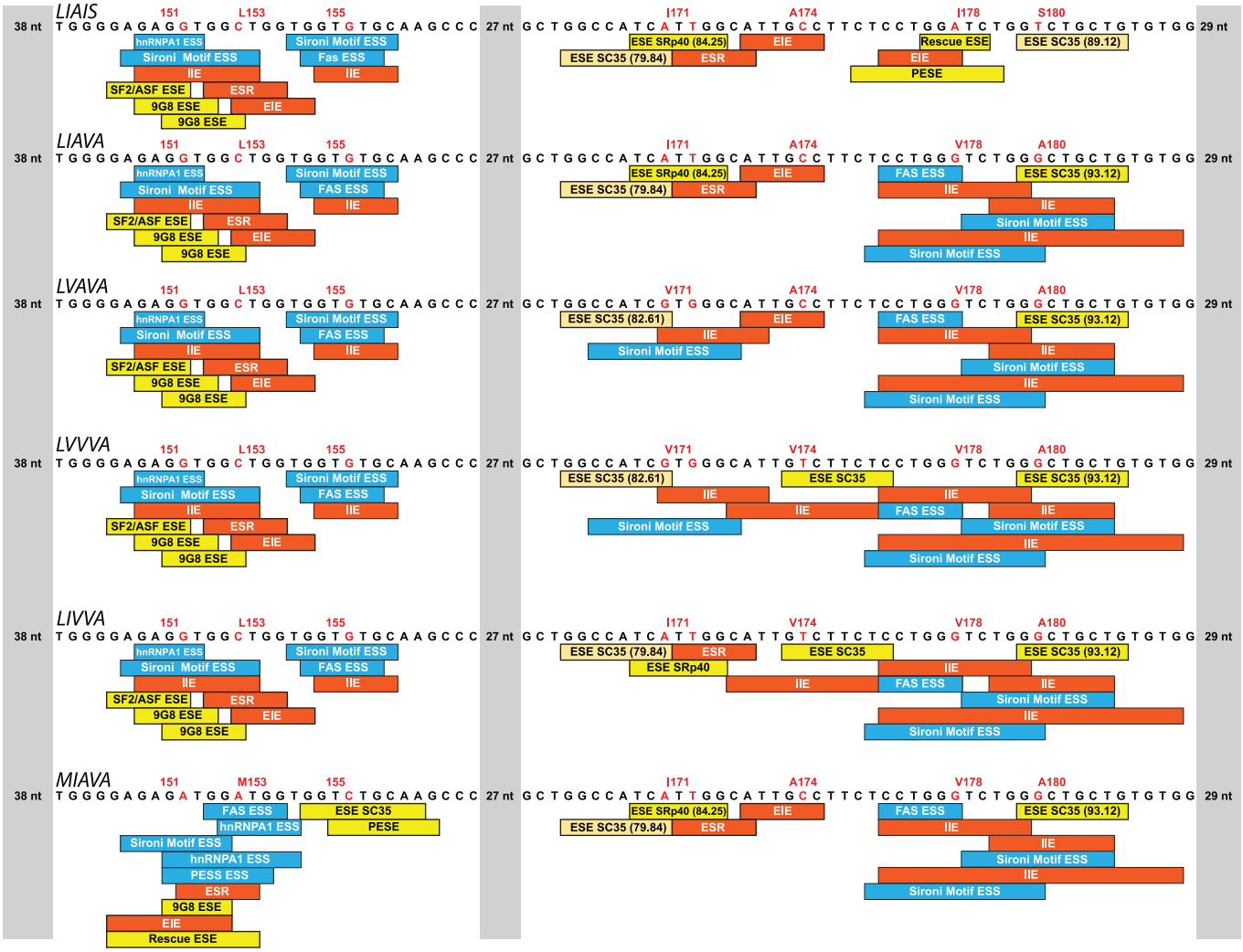

Figure 7. Changing landscape of ESRs in exon 3 of the human *L* and *M* opsin genes with polymorphisms in codons 151, 153, 155, 171, 174, 178, and 180 identified by HSF 3.0. Exon 3 is comprised of 169 nucleotides. The identities of the first 38 nucleotides, the last 29 nucleotides and 27 nucleotides encompassing codons 159 through 167 are not shown. Codons 151, 153, 155, 171, 174, 178, 180 are identified as are the amino acids encoded by each of the variants shown, which are, from top to bottom: *LIAIS*, *LIAVA*, *LVAVA*, *LIVVA*, *LVVVA*, and *MIAVA*. The variant nucleotide positions are cDNA nucleotide numbers 453 (codon 151), 457 (codon 153), 465 (codon 155), 511 and 513 (codon 171), 521 (codon 174), 532 (codon 178), and 538 (codon 180). The nucleotides above the *blue boxes* were identified by HSF as motifs that function as splicing silencers, and the nucleotides above the *yellow boxes* were identified as motifs that function as splicing enhancers. ESE SC35 motifs that are present across all the variants shown, but have variable consensus threshold values, are indicated by slightly different *yellow boxes* and the consensus value thresholds are given in *parenthesis* within the box. The nucleotides above the *red boxes* were identified as motifs that regulate splicing but that can function as silencers or enhancers, depending on the context. Here, motifs labeled IIE were identified as silencers, and motifs identified as EIE or ESR were identified as enhancers. There are multiple overlapping enhancers motifs for SR protein binding in nucleotides 522 through 531 that are constant across all variants shown, and these are not indicated in the Figure.

might be achievable in individuals, such as 11-0271, who suffer from blue cone monochromacy because all of their L/M cones are nonfunctional due to the splicing defect. It would be of interest to know whether gene therapy administered early in life could prevent the high-grade myopia phenotype of subjects with an *LIAVA* gene and a normal *L* or *M* opsin gene.

LVAVA Opsin Variant Defective at Level of Pre-mRNA Splicing and Protein Structure/Function

Both 10-0059 and 11-0115 have a single opsin gene on the X-chromosome, and in both subjects it encodes an *LVAVA* L/M interchange opsin. These subjects

have a clear, but greatly diminished *L/M* cone ERG (Fig. 2A). The minigene assay also indicates that the *LVAVA* opsin has a splicing defect similar to the *LIAVA* variant discussed above, but the splicing defect is incomplete for the *LVAVA* variant. A small amount of full-length mRNA was observed in the minigene assay, and the ERG results indicated that a small amount of functional photopigment is made. Just as was observed for the *LIAVA* splicing defect, the *LVAVA* splicing defect arises through a failure of exon 3 to be recognized as an exon, and, therefore, it is skipped when the pre-mRNA is processed, instead exon 2 is spliced directly to exon 4, and the mRNA is likely degraded in the nonsense-mediated decay pathway.

Previous adaptive optics and optical coherence tomography imaging of the retinas of subjects 10-0059 and 11-0115 showed severe foveal disruption consistent with cone degeneration (10-0059 was JC_0347 and 11-0115 was JC_0564 in the prior study).[14] Here we demonstrated that these subjects do not have measurable *S* cone ERGs, consistent with degeneration seen in the prior imaging studies. The fact that the coding regions, the intron/exon junctions, and the promoter of the S opsin genes are normal in these subjects makes it extremely unlikely that a mutation in the S opsin gene accounts for the absence of S cone function.

The results from mice in this study provided evidence that there is a defect in protein structure and function in the LVAVA opsins. The *L/M* cone ERG responses were reduced by approximately 50% in the $Opn1lw^{LVAVA}$ mice compared to the ^{OPN1lwLIAIS} mice (Fig. 4), and this was true for every time point examined. Further clues about the nature of the defect come from the observation illustrated in Figure 5 that the outer segment of cones from 3-month-old *LVAVA* mice show much less opsin staining compared to 3-month-old *LIAVA* and *LIAIS* mice. These observations are consistent with the conclusion that there is a defect either in protein folding or in trafficking of the *LVAVA* opsin to the cone outer segment. Taken together, the mouse and human results suggested that the cone phenotype in humans with an *LVAVA L/M* interchange opsin gene is due to a combination of incorrect splicing and defects at the protein level. The splicing defect leads to the production of only a very small amount of functional photopigment, while toxic effects caused by protein folding or trafficking of the small amount of LVAVA opsin that is made leads to L/M cone degeneration. S cones degenerate most likely secondarily due to a by-stander effect.

For the variants *LIAIS*, *LIAVA*, *LVAVA*, *LIVVA*, and LVVVA, only the nucleotide variations in codons 171, 174, 178, and 180 have a role. Splicing can be affected directly by sequence alterations in exonic regulators of splicing or indirectly by effects on secondary structure that alter accessibility of *trans*-acting splicing factors to *cis*-elements. An analysis of the effects of the nucleotide differences between the *LIAIS* and *LIAVA* variants using the RNAsnp webtool indicated no significant effect on secondary structure ($P = 0.41$),[43] suggesting that the landscape of splicing enhancers and silencers are responsible for exon skipping. The region encompassing codons 171 through 180 of the *LIAIS* variant is populated by enhancer motifs, and no silencer motifs are present. The *LIAIS* variant includes exon 3 in the mRNA approximately 100% of the time. Changes in codons 178 and 180 that accompany the *LIAVA* variant prevent exon 3 inclusion in the mRNA, create several silencer motifs, destroy three enhancer motifs, and slightly increases the threshold for the fourth enhancer motif. Thus, the silencers spanning codons 178 to 180 must abolish exon 3 inclusion. The *LVAVA* variant differs from the *LIAVA* variant only in codon 171. This change is accompanied by a slight rescue of the splicing defect compared to *LIAVA*, as evidenced by the minigene assay and by ERG results for human subjects. This suggests that the enhancers that span codon 171 when isoleucine is specified at codon 171 do not function as regulators of splicing, perhaps due to antagonistic interactions between the SRp40 and SC35 binding motifs, as has been observed in other systems.[44] When valine is specified at codon 171, the strength of the SC35 consensus value threshold is increased, the SRp40 binding motif is absent, and two silencer motifs (Sironi motif, and IIE) are created. The observation that exon 3 is included in the mRNA some of the time for the *LVAVA* variant but not for the *LIAVA* variant suggests that the change in the enhancers have an effect, but the addition of the silencers do not.

The only difference between the *LVAVA* and *LVVVA* minigenes examined here is in codon 174 and Figure 6 shows that this change markedly rescues exon 3 skipping. The change in codon 171 from GCC to GTC creates an SC35 enhancer motif, abolishes an EIE enhancer, and creates a silencer motif (IIE). The fact that this change is accompanied by a dramatic rescue in the splicing defect, suggests that the added IIE either does not function as a silencer or that it is offset by the SC35 enhancer motif so the net effect is enhancement of normal splicing.

The above described scenario for enhancer and silencer functions at codon 171 predicts that changing *LVVVA* to *LIVVA* should dramatically reduce exon 3 inclusion because when only the SC35 (consensus threshold value 82.61) is present, exon 3 is included, but when the combination of the SRp40 motif, an SC35 motif with consensus value of 79.84, and an ESR motif all are present, enhancer activity is blocked. This prediction matches what was observed in the minigene assay for *LIVVA*, which shows nearly complete exon 3 skipping in comparison with *LVVVA* (Fig. 6).

The observation that silencers encompassing codons 178 and 180 completely block exon 3 inclusion in *LIAVA* compared to *LIAIS* suggests that changing *LIAVA* to *LIAVS* might rescue the splicing defect to some degree. This effect was observed in the minigene assay (Fig. 6). The *LIAVS* mutation was previously identified in multiple members of two families who had it as the only X-chromosome cone opsin gene, and the phenotype included mild myopia (SER ranged −1.75 to −5.00) and a measurable flicker photometric (fp)-ERG compared to *LIAVA* subjects in the same study who had high grade myopia (SER −6.00 and −18.00) and no measurable fp-ERG.[13] Adaptive optics and OCT imaging of one of the LIAVS subjects revealed a severely disrupted fovea.[14] Overall, imaging results have shown that the *LIAVA* opsin gene has a complete splicing defect so that no detectable functional photopigment is made and it has a milder retinal phenotype than any of the opsin variants that exhibit a partial splicing defect so that photoreceptors contain a reduced amount of functional protein compared to normal (as evidenced by reduced ERG b-wave amplitudes). Evidence from mice in this study revealed that the LVAVA photopigment exhibits toxicity at the level of protein likely due to folding or trafficking abnormalities, but whether the LIAVS and LVVVA photopigments also exhibit similar protein abnormalities remains to be seen. The retinal phenotypes might suggest that, indeed, these photopigments are toxic.

It has been reported that in addition to the exon 3 skipped mRNA there is a smaller mRNA that is missing the 3′ 72 nucleotides from exon 2 in addition to missing exon 3.[45] which was not observed in this study. Deletion of the last 72 nucleotides of exon 2 places a new splice site in codon 113, with a splice site between cDNA residues 337 and 338. Human *OPN1LW* and *OPN1MW* genes are variable at exon 2 codons 65, 100, 111, and 116 (cDNA residues c.194C>T, c.300A>G, c.331A>G, c.347C>A). The exon 2 CAAC haplotype is most typical of *OPN1LW* genes, and the TGGA haplotype is most typical of *OPN1MW* genes. The subjects studied here all had the CAAC exon 2 haplotype. HSF analysis of the two exon 2 haplotypes reveals that a new splice donor is created when c.331 is G such that the new splice site is between residues 333 and 334 (GTT gtgacc, where upper case is recognized as the new 3′ end of exon 2 and the lower case letters are exon 2 sequences that are now recognized as intron). In addition, this change creates a new Sironi silencer motif and a binding site for the protein hnRNPA1 which is an exonic splice silencer. These results suggested that exon 2 polymorphisms also may have a role in splicing. The TGGA exon 2 haplotype may be responsible for the deletion of the extra 72 nucleotides from the 3′ end of exon 2 observed by Buena-Atienza et al.[45] and this may explain why we did not observe it here.

How Do the Exon 3-Skipping Cone Opsin Mutants Contribute to Myopia?

The understanding of how *LVAVA* and *LIAVA* opsin gene variants affect cone function provides new insight into the mechanism responsible for myopia. *LVAVA* is the causative mutation at *MYP1*, the first identified high-grade myopia locus (OMIM 310460), and the phenotype has been designated BED.[43] The BED phenotype, caused by having a submosaic of *L*/*M* cones that express an *LVAVA* opsin gene, includes extremely high-grade myopia, astigmatism, and an abnormal cone ERG. The *LIAVA* opsin gene variant also has been associated with myopia[18] and the *LIAVA* patient reported here expressing an *LIAVA* opsin gene in all of his cones has −15.25 diopters of myopia.

When emmetropization occurs normally, changes in the pattern of light and dark in the image that characterize blurred versus sharply focused images are monitored by the retina to control eye growth so that its adult length matches the focal length of its optics. Presumably, the high myopia associated with the *LVAVA* and *LIAVA* opsin genes can be explained by a disruption of the signals that guide emmetropization, which are initiated by light absorption in the photopigments expressed in the *L* and *M* cones.

The first evidence that axial growth associated with myopia is controlled by the retina came from studies in which lid suture in monkeys caused myopia. Lid suturing prevents pattern vision, while only modestly reducing the amount of light reaching the cones;[46] thus, it has become widely accepted that in normal

childhood development, blurry images associated with hyperopia stimulate axial elongation and the "function of emmetropization is to minimize blur."[47] The blur hypothesis has been a critically important theory in the field of refractive error, and accordingly, many strategies for myopia prevention have focused on corrective lenses that might reduce the amount of blur, for example, in the periphery,[48] or under certain circumstances, that is, during accommodation.[49]

The effects of mutations in the L and M opsins and their associations with myopia indicate a very different understanding of how contrast mechanisms in the retina may be involved in controlling eye growth during emmetropization. First, there appears to be a strong association between the number of cones expressing the *LIAVA* opsin gene and the degree of myopia. Among the patients with the *LIAVA* opsin gene reported by Patterson et al.,[18] those with relatively few cones expressing *LIAVA* had emmetropic or nearly emmetropic vision while those with the fewest normal cones had high myopia. Thus, there was a statistically significant correlation between the relative number of visible, wave guiding cones and refractive error. Consistent with that trend, patient 11-0271 reported here as expressing the *LIAVA* opsin gene in all *L/M* cones had a very large refractive error (–15.25). Similarly, two patients reported by Buena-Atienza et al.[45] had opsin gene arrays that carried a single gene, and the gene specified the *LIAVA* variant and they had refractive errors of −12 and −14 diopters, respectively. Buena-Atienza et al.[45] also note the trend that among individuals expressing a single mutant opsin gene, myopia tends to be more severe in patients with the *LIAVA* opsin gene, compared to patients with the *LVAVA* opsin gene.

The *LIAVA* patients with the largest refractive errors are similar in their extremely high myopia to patients with mutations in the nyctalopin gene (*NYX*),[50] which causes insensitivity to glutamate released by photoreceptors to ON-bipolar cells. Bipolar cells have center-surround receptive fields that are activated by contrast, as produced by sharply focused images, and are less active in response to blurry images in which light is spread evenly across the receptive field. Glutamate acts as an inhibitory neurotransmitter for ON-bipolar cells and, thus, *NYX* mutations cause them to be constitutively activated, constantly signaling high contrast, suggesting, contrary to the blur hypothesis, that contrast stimulates axial elongation.

NYX mutations cause an insensitivity to glutamate even though it is being released. Patients with an *LIAVA* opsin gene clearly have cone inner segments[14] where sodium is pumped out of the photoreceptor, but they lack photopigment and visible outer segments where the cation channels required for depolarization are normally located. Thus, they are expected to be constitutively hyperpolarized, preventing release of glutamate required to inhibit ON bipolar cells. This would explain the correlation between the number of *LIAVA* expressing cones and myopia; the greater numbers of defective cones that cannot release glutamate normally in the dark, the greater the disinhibition of ON-bipolar signaling, which is responsible for signaling the eye to grow.

This also could explain why patients who express an *LVAVA* opsin gene in all L/M cones have a lower degree of myopia than those BED patients who express *LVAVA* in only a submosaic of cones. Unlike *LIAVA* expressing cones, *LVAVA* expressing cones function and might be expected to release nearly normal levels of glutamate in the dark, suppressing ON bipolar cell activity. However, in the light, a normal cone adjacent to low functioning LVAVA cones would be relatively hyperpolarized even in the presence of nearly uniform illumination across the receptive field as produced by blurred images. The constitutive "contrast" between normal cones and "LVAVA" cones would activate ON-bipolar cells, stimulating abnormal axial elongation explaining high myopia in Bornholm eye disease patients.

The activity of the ON bipolar cells, which we suggest is the signal for axial elongation, is controlled by the hyperpolarization of the cone terminal. Normally, light on a cone hyperpolarizes it, but this can be counteracted by feedback from neighboring cones that are also light activated under conditions of uniform illumination. The ideal stimulus for complete shut-off of glutamate and maximum stimulation of ON-bipolar cells, and theoretically, maximum stimulation of axial elongation, is maximum light on a central cone and minimal light on neighboring cones as produced by very high contrast, high spatial frequency, and well-focused images. This could explain why excessive reading of high contrast text causes myopia.

What remains to be explained, according to this idea, is myopia that occurs under conditions in which the contrast across the mosaic is minimal, such as myopia associated with diffusers. One factor that must come into play is contrast adaptation, a phenomenon in which the gain of the contrast detector is increased after prolonged exposure to

low contrast stimuli. The presence of light but little contrast may result in increases in contrast gain explaining the myopia induction by diffusers. This also would explain why rearing lid sutured animals in the dark leads to hyperopia rather than myopia.[46] The constant release of glutamate in the dark would silence the ON bipolar cells and prevent axial elongation.

We suggest that the idea that "contrast" is the driver for axial elongation deserves consideration as an alternative to the "blur" hypothesis. It could explain many aspects of myopia including the dramatic escalation of myopia associated with increasing urbanization, less outdoor activity, increased emphasis on academic success, and the use of video screens in education, social activity, entertainment, and recreation. For example, it is well established that axial elongation is a local effect, and the peripheral retina is important for controlling it.[48] Compared to modern children, for Paleolithic children, accommodation occurred outdoors when they were interacting with friends and family at close distances or manipulating an object, such as a tool or toy held in the hands and imaged on the fovea. The images of the close-up objects are focused on the central retina but the background outdoor scene in the distance fills peripheral vision. For young children whose eyes still are developing and, therefore, hyperopic or "far-sighted," the distant background of an outdoor scene remains somewhat in focus even when they are accommodating to more close-up objects viewed in the fovea. However, as the eye grows to emmetropia, distance objects imaged in the periphery will become more blurry when the eye is accommodated. Thus, contrary to the "blur hypothesis," which proposed that the eye grows to clarity, we argue that the function of emmetropization is for the eye to grow until far-away images in the periphery become blurry because they are no longer as well focused under the normal state of accommodation to near objects imaged on the fovea. Accordingly, computers, television, tablets, and other screens cause myopia because they fill peripheral vision with well-focused images when the eye is accommodated, signaling the eye to grow.

Myopia is a significant public health concern and it is critical that new treatment strategies for myopia be developed.[51,52] Optical treatment regimens for slowing myopia based on the blur hypothesis have had limited success. New treatments for slowing myopia progression promise to come from insights into the etiology of myopia gained from results from human patients with myopia associated with mutations in genes expressed in the retina as reported here.

Acknowledgments

Supported by National Institutes of Health (NIH; Bethesda, MD) Grants R01EY021242, R01EY009620, and P30EY001730; Vision Training Grant T32EY07031; the Research to Prevent Blindness; the Bishop Foundation; the Ray H. Hill Foundation; and the Tietze Foundation.

Disclosure: **S.H. Greenwald**, None; **J.A. Kuchenbecker**, None; **J.S. Rowlan**, None; **J. Neitz**, None; **M. Neitz**, None

References

1. Parmley JL, Urrutia AO, Potrzebowski L, et al. Splicing and the evolution of proteins in mammals. *PLoS Biol*. 2007;5:e14.
2. Ward AJ, Cooper TA. The pathobiology of splicing. *J Pathol*. 2010;220:152–163.
3. Sterne-Weiler T, Sanford JR. Exon identity crisis: disease-causing mutations that disrupt the splicing code. *Genome Biol*. 2014;15:201.
4. Sterne-Weiler T, Howard J, Mort M, et al. Loss of exon identity is a common mechanism of human inherited disease. *Genome Res*. 2011;21:1563–1571.
5. Stergachis AB, Haugen E, Shafer A, et al. Exonic transcription factor binding directs codon choice and affects protein evolution. *Science*. 2013;342:1367–1372.
6. Neitz J, Neitz M. The Genetics of normal and defective color vision. *Vis Res*. 2011;51:633–651.
7. Nathans J, Piantanida TP, Eddy RL, et al. Molecular genetics of inherited variation in human color vision. *Science*. 1986;232:203–210.
8. Neitz M, Neitz J, Grishok A. Polymorphism in the number of genes encoding long-wavelength sensitive cone pigments among males with normal color vision. *Vis Res*. 1995;35:2395–407.
9. Verrelli BC, Tishkoff SA. Signatures of selection and gene conversion associated with human color vision variation. *Am J Hum Genet*. 2004;75:363–375.
10. Carroll J, Neitz M, Hofer H, et al. Functional photoreceptor loss revealed with adaptive optics:

an alternate cause of color blindness. *Proc Natl Acad Sci. U S A*. 2004;101:8461–8466.
11. Crognale MA, Fry M, Highsmith J, et al. Characterization of a novel form of X-linked incomplete achromatopsia. *Vis Neurosci*. 2004;21: 197–204.
12. Neitz M, Carroll J, Renner A, et al. Variety of genotypes in males diagnosed as dichromatic on a conventional clinical anomaloscope. *Vis Neurosci*. 2004;21:205–216.
13. Mizrahi-Meissonnier L, Merin S, Banin E, et al. Variable retinal phenotypes caused by mutations in the X-linked photopigment gene array. *Invest Ophthalmol Vis Sci*. 2010;51(8):3884–3892.
14. Carroll J, Dubra A, Gardner JC, et al. The effect of cone opsin mutations on retinal structure and the integrity of the photoreceptor mosaic. *Invest Ophthalmol Vis Sci*. 2012;53:8006–8015.
15. Ueyama H, Muraki-Oda S, Yamade S, et al. Unique haplotype in exon 3 of cone opsin mRNA affects splicing of its precursor, leading to congenital color vision defect. *Biochem Biophys Res Commun*. 2012;424:152–157.
16. McClements M, Davies WI, Michaelides M, et al. Variations in opsin coding sequences cause x-linked cone dysfunction syndrome with myopia and dichromacy. *Invest Ophthalmol Vis Sci*. 2013; 54:1361–1369.
17. Gardner JC, Liew G, Quan YH, et al. Three different cone opsin gene array mutational mechanisms with genotype-phenotype correlation and functional investigation of cone opsin variants. *Hum Mut*. 2014;35:1354–1362.
18. Patterson EJ, Wilk M, Langlo CS, et al. Cone photoreceptor structure in patients with X-linked cone dysfunction and red-green color vision deficiency. *Invest Ophthalmol Vis Sci*. 2016;57: 3853–3863.
19. Winderickx J, Battisti L, Motulsky AG, et al. Selective expression of human X chromosome-linked green opsin genes. *Proc Natl Acad Sci U S A*. 1992;89:9710–9714.
20. Li J, Gao B, Guan L, et al. Unique variants in OPN1LW cause both syndromic and nonsyndromic X-linked high myopia mapped to MYP1. *Invest Ophthalmol Vis Sci*. 2015;56:4150–4155.
21. Vaithinathan R, Berson EL, Dryja TP. Further screening of the rhodopsin gene in patients with autosomal dominant retinitis pigmentosa. *Genomics*. 1994;21:461–463.
22. Ayuso C, Trujillo MJ, Robledo M, et al. Novel rhodopsin mutation in an autosomal dominant retinitis pigmentosa family: phenotypic variation in both heterozygote and homozygote Val137Met mutant patients. *Hum Genet*. 1996;98:51–54.
23. McMahon C, Neitz J, Neitz M. Evaluating the human X-chromosome pigment gene promoter sequences as predictors of *L*:*M* cone ratio variation. *J Vision*. 2004;4:203–208.
24. Davidoff C, Neitz M, Neitz J. Genetic testing as a new standard for clinical diagnosis of color vision deficiencies. *Trans Vis Sci Technol*. 2016;5:2.
25. Gunther KL, Neitz J, Neitz M. A novel missense mutation in the S cone photopigment in a male who made Tritan errors on the Neitz Test of Color Vision. *Invest Ophthalmol Vis Sci*. 2003; 44(suppl):B803–B03.
26. Baraas RC, Hagen LA, Dees EW, et al. Substitution of isoleucine for threonine at position 190 of S-opsin causes S-cone-function abnormalities. *Vis Res*. 2012;73:1–9.
27. Greenwald S, Kuchenbecker JA, Roberson RK, et al. S-opsin knockout mice with the endogenous *M*-opsin gene replaced by an *L*-opsin variant. *Vis Neurosci*. 2014;31:25–37.
28. Nathans J, Thomas D, Hogness DS. Molecular genetics of human color vision: the genes encoding blue, green, and red pigments. *Science*. 1986;232:193–202.
29. Röhlich P, van Veen T, Szél Á. Two different visual pigments in one retinal cone cell. *Neuron*. 1994;13:1159–1166.
30. Applebury ML, Antoch MP, Baxter LC, et al. The murine cone photoreceptor: a single cone type expresses both S and M opsins with retinal spatial patterning. *Neuron*. 2000;27:513–523.
31. Haverkamp S, Wassle H, Duebel J, et al. The primordial, blue-cone color system of the mouse retina. *J Neurosci*. 2005;25:5438–5445.
32. Kuchenbecker JA, Greenwald S, Neitz M, et al. Cone-isolating ON-OFF electroretinogram for studying chromatic pathways in the retina. *J Opt Soc Am A*. 2014;31:A208–A213.
33. Bush RA, Sieving PA. Inner retinal contributions to the primate photopic fast flicker electroretinogram. *J Opt Soc Am A*. 1996;13:557–565.
34. Schneider CA, Rasband WS, Eliceiri KW. NIH Image to ImageJ: 25 years of image analysis. *Nat Methods*. 2012;9:671–675.
35. Desmet FO, Hamroun D, Lalande M, et al. Human Splicing Finder: an online bioinformatics tool to predict splicing signals. *Nucl Acids Res*. 2009;37:e67.
36. Neitz M, Neitz J. A new test for mass screening of school age children for red-green color vision defects. *Color Res Appl*. 2001;26(S1):S239–S249.

37. Dacey DM, Packer OS. Colour coding in the primate retina: diverse cell types and cone-specific circuitry. *Curr Opin Neurobiol*. 2003;13:421–27.
38. Hofer H, Carroll J, Neitz J, et al. Organization of the human trichromatic cone mosaic. *J Neurosci*. 2005;25:9669–9679.
39. Gresh J, Goletz PW, Crouch RK, et al. Structure-function analysis of rods and cones in juvenile, adult, and aged C57bl/6 and Balb/c mice. *Vis Neurosci*. 2003;20:211–220.
40. Zhang C, Li WH, Krainer AR, et al. RNA landscape of evolution for optimal exon and intron discrimination. *Proc Natl Acad Sci U S A*. 2008;105:5797–802.
41. Chang B, Mandal MN, Chavali VR, et al. Age-related retinal degeneration (arrd2) in a novel mouse model due to a nonsense mutation in the Mdm1 gene. *Hum Mol Genet*. 2008;17:3929–3941.
42. Nguyen LS, Wilkinson MF, Gecz J. Nonsense-mediated mRNA decay: inter-individual variability and human disease. *Neurosci Biobehav Rev*. 2014;46(Pt 2):175–186.
43. Sabarinathan R, Tafer H, Seemann SE, et al. The RNAsnp web server: predicting SNP effects on local RNA secondary structure. *Nucleic Acids Res*. 2013;41:W475–479.
44. Chandradas S, Deikus G, Tardos JG, et al. Antagonistic roles of four SR proteins in the biosynthesis of alternatively spliced tissue factor transcripts in monocytic cells. *J Leuk Biol*. 2010; 87:147–152.
45. Buena-Atienza E, Ruther K, Baumann B, et al. De novo intrachromosomal gene conversion from OPN1MW to OPN1LW in the male germline results in Blue Cone Monochromacy. *Sci Rep*. 2016;6:28253.
46. Wiesel TN, Raviola E. Myopia and eye enlargement after neonatal lid fusion in monkeys. *Nature*. 1977;266:66–68.
47. Wallman J, Winawer J. Homeostasis of eye growth and the question of myopia. *Neuron*. 2004;43:447–468.
48. Smith EL III. Prentice Award Lecture 2010: a case for peripheral optical treatment strategies for myopia. *Optom Vis Sci*. 2011;88:1029–1044.
49. Gwiazda J, Hyman L, Hussin HM, et al. A randomized clinical trial of progressive addition lenses versus single vision lenses on the progression of myopia in children. *Invest Ophthalmol Vis Sci*. 2003;44:1492–500.
50. Zhang Q, Xiao X, Li S, et al. Mutations in NYX of individuals with high myopia, but without night blindness. *Mol Vis*. 2007;13:330–336.
51. Holden BA, Jong M, Davis S, et al. Nearly 1 billion myopes at risk of myopia-related sight-threatening conditions by 2050 - time to act now. *Clin Exp Optom*. 2015;98(6):491–493.
52. Holden BA, Fricke TR, Wilson DA, et al. Global prevalence of myopia and high myopia and temporal trends from 2000 through 2050. *Ophthalmology*. 2016;123:1036–42.